Non-cooled near infrared spectroscopy

Richard Dallier, Jean-Gabriel Cuby

Non-cooled near infrared spectroscopy

R. Dallier[a,c] and J.G. Cuby[b,c]

[a]CRPE – Ecole des Mines de Nantes, 4 rue Alfred Kastler
B.P. 20722, 44307 Nantes cedex 3, France

[b]ESO, Karl–Schwarzschild Str.2, D–85748 Garching, Germany

[c]Visiting astronomer, Canada–France–Hawaii Telescope operated by the
National Research Council of Canada, the Centre National de la Recherche Scientifique
de France and the University of Hawaii

ABSTRACT

We investigate the use of non-cryogenic instrumentation for near infrared spectroscopy. With this technique, it is possible to apply in the J and H bands some instrument concepts and observing techniques used in the visible. We present observations of the thermal background in H. We derive some instrument requirements for minimizing and handling it. We recommend the use of short wavelength cutoff wavelengths or linear filters in H. We present observations of the sky emission, and do confirm previous upper limits of the continuum emission between the OH lines. We discuss some applications of non-cooled near infrared spectroscopy.

Keywords: Near Infrared, spectroscopy, OH airglow, thermal background

1. INTRODUCTION

The growing availability of near IR detectors of large format, low dark current and readout noise brings new observing capabilities of the universe, both in imaging and spectroscopy. The much lower absorption of light in the IR allows the study in this domain of heavily obscured regions (star forming regions, galaxy centers etc.). The redshift effect makes the near IR bands the window of choice for the observation of distant galaxies at redshifts above ~ 1, for which most of the emission and absorption lines present in the galaxy spectra disappear from the visible. The near IR domain also allows specific physical diagnostics via the observation of spectral signatures, most of them molecular, present in the IR.

As a consequence, instrumental requirements in the near IR are increasing, pushing for more instrumental flexibility, observing modes and capabilities. Because cryogenic designs put severe limitations on versatility, it is tempting to work in the near IR as in the visible, with only the detector being cooled, and the rest of the instrument warm. Not cooling the whole instrument, but only the detectors, as for visible instruments, allows more configuration flexibility and more observing capabilities. Among the most rewarding applications that can be foreseen in extending visible concepts to the near infrared is multi-object spectroscopy, either with masks or fibres. We will subsequently refer to this mode of operation as 'non-cooled near infrared spectroscopy'. The aim of this paper is to quantify the intrinsic limitations and performances of the technique imposed by the specifics of the near IR domain, i.e. OH sky emission and thermal background.

The long wavelength edge of the visible spectrum is usually considered to be ~ 1 μm because of the silicon cutoff at this wavelength. Astronomical instruments working above this limit rely most of the time on cryogenic designs, with detectors covering huge spectral ranges, generally up to 2.5 or 5 μm. With the development during the past decade of new technology detectors whose performances and characteristics are steadily approaching those of silicon CCDs, technical concepts in the near infrared are evolving towards visible ones.

It is well known that the sky emission above ~ 2.2 μm is essentially limited by thermal emission, whereas below this limit OH airglow emission dominates. This turnoff in the spectral energy distribution of the background is generally considered as the upper limit of the operating wavelength of non-cooled instrumentation in the near IR. This is usually derived from figures similar to the dashed lines of figure 1 (see e.g. Ref. 1). These dashed lines

represent the mean sky fluxes in the J, H and K bands, and the thermal background as detected with a cooled spectrometer (T = 273 K and 20% emissivity on the figure). The situation is indeed more complex, and the 'cutoff' wavelength in non-cooled spectroscopy is actually much lower, and, depending on the application, lies between 1.4 and 1.8 μm. The reason is that the background is not dispersed in a non-cooled instrument, but actually consists in the integrated part of the blackbody spectral energy distribution, usually seen with an emissivity of 100%, over the observing band. This explains why the dashed lines of figure 1, derived from observations carried out with cryogenic instruments, is not representative of the non-cooled case.

The thermal background contribution in the non-cooled case is shown with a solid line in figure 1, assuming a temperature of 273 K and an emissivity of 100 per cent.

When now accounting for the discrete structure of the OH emission, rather than for the mean fluxes, it clearly turns out from figure 1 that with a non-cooled instrument, at the spectral resolution of the figure (800 per pixel), the thermal background becomes the dominant source of noise if observing *between* the OH lines above $\sim$ 1.6 μm, while emission on the lines still dominates up to $\sim$ 1.9 μm. Clearly, thermal background in K with a non-cooled spectrometer is totally dominating, preventing high performance observations in this band. Note also that the integrated background curve (solid line) in a non-cooled instrument is not modified when the spectral resolution changes, whereas the dispersed background curve (dashed line) with a cryogenic instrument varies linearly with the spectral resolution.

We describe our observations in section 2. Then, we discuss the thermal background in the H band in section 3. In section 4, we present our observations of the continuum emission between OH lines. In section 5, we consider some potential applications of the technique.

2. OBSERVATIONS

The measurements of the thermal background and of the airglow spectrum reported in this paper are a by-product of observations carried out at CFHT with a visitor instrument, ISIS–IR, developed at Observatoire de Paris, and working in the J and H bands. This instrument consists in a 50 fibre image dissector and in a bench grating spectrograph providing resolving powers up to $\sim$ 2,000. Preliminary versions of this instrument are described in Ref. 4. The instrument uses one of the two CFHT Nicmos cameras, Redeye Wide which provides a demagnification factor of 1.7::1.0 (see Ref. 5 and http://www.cfht.hawaii.edu). The fibre bundle at the focal plane of the telescope covers a field of view of $\sim$ 7 arcsec at the direct f/8 focus, and of $\sim$ 12 arcsec with the use of a focal reducer. The fibres are aligned at the other end of the bundle and form the entrance slit of the spectrograph. Flat field spectra and comparison lamp spectra are taken via the telescope calibration unit located in the Cassegrain adapter. The fibre to fibre transmission is calibrated on flat fields or by flux scaling on well isolated OH airglow lines. Data reduction procedures have been developed under IRAF.
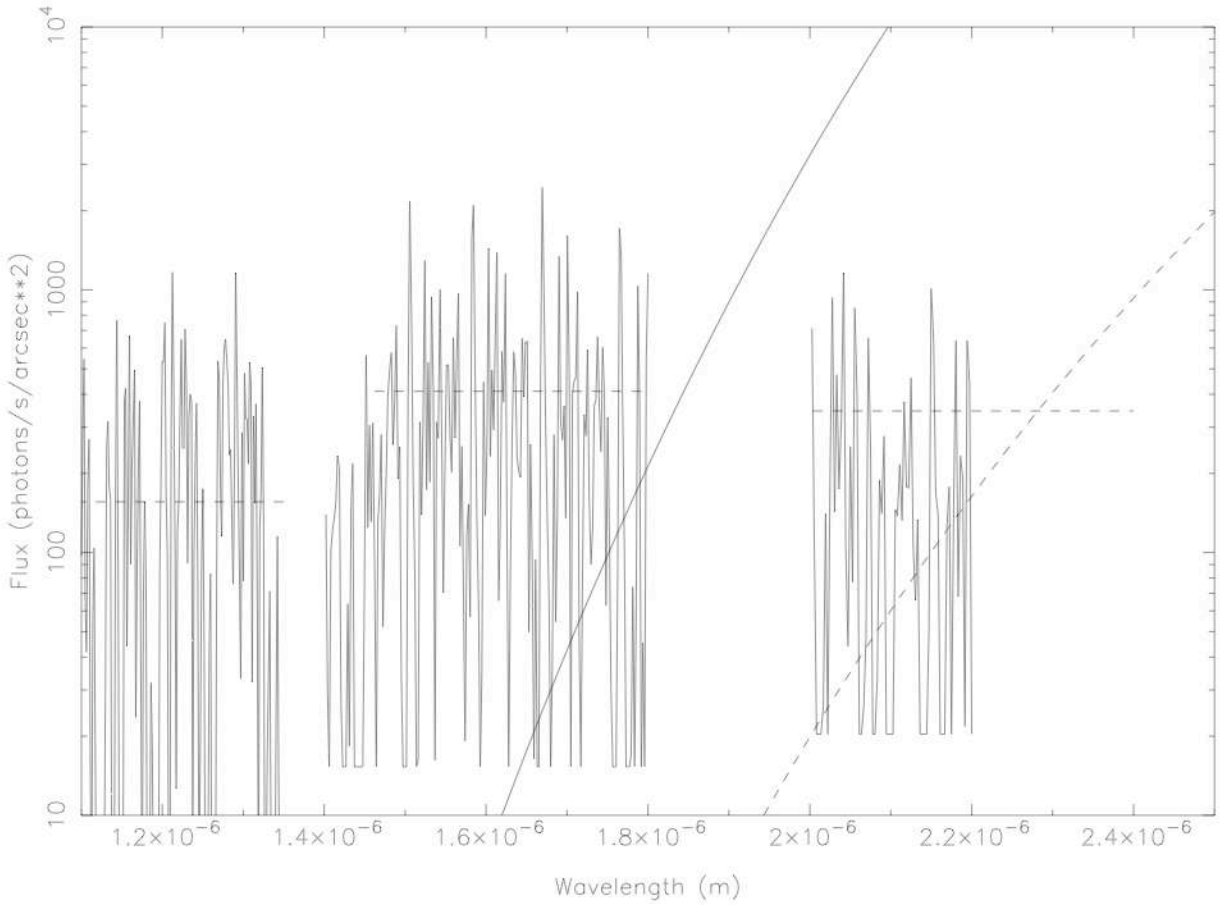
3. THERMAL BACKGROUND

3.1. Introduction

In a cryogenic spectrograph, the background is dispersed and at moderately low emissivity (within the atmospheric transmission windows). It is simply given by the following expression[1]:

$$N^{\mathrm{TB}}(\lambda) = A\,\Omega\,\eta_{\mathrm{ins}}\,\epsilon\,\mathcal{F}(\lambda)\,\frac{2c}{\lambda^3\,\exp\frac{hc}{\lambda kT}-1}\,\frac{1}{R} \qquad (1)$$

with N^{TB} the number of thermal background electrons per second and per pixel, A is the telescope area, Ω the solid angle at which a pixel sees the telescope pupil, η_{ins} the instrument transmission, ϵ the atmosphere + telescope emissivity, $\mathcal{F}(\lambda)$ the filter spectral transmission curve, λ the wavelength, T the site temperature and R the resolving power per pixel.

In the non-cooled case, the behavior is different, since the slit environment is warm. In this case, the background is no longer at low emissivity, nor dispersed. Let us consider for instance the slit jaws which radiate at room temperature with an emissivity of 100%. After the dispersing element, all the points of the slit jaws generate spectra which overlap onto the detector, re-forming an integrated background. This situation is exactly similar to re-forming an integrated sky background in slitless spectroscopy (e.g. objective prisms). The rest of the 'warm' optics also

Figure 1. Spectral energy distribution of the sky (OH lines and continuum) and thermal backgrounds in the near infrared on a 4m telescope. The resolution is 800 per pixel. The OH line fluxes have been scaled so as to give integrated magnitudes of 16 in J and 14.5 in H. The continuum levels between the lines are from Ref. 2 in J and from Ref. 3 in H. The parameters in K are somewhat arbitrary as no data is available for the continuum between the lines. The structured solid line shows the OH spectrum. The solid line at the middle of the figure represents the thermal background corresponding to T = 273 K and 100% emissivity, integrated from $\sim 1\mu m$ to the wavelength reported in the horizontal axis. The horizontal dashed lines correspond to the mean magnitudes in J (16), H (14.5) and K (14). The dashed line on the right of the figure shows a dispersed thermal background at R = 800 per pixel, T = 273 K, and 20% emissivity.
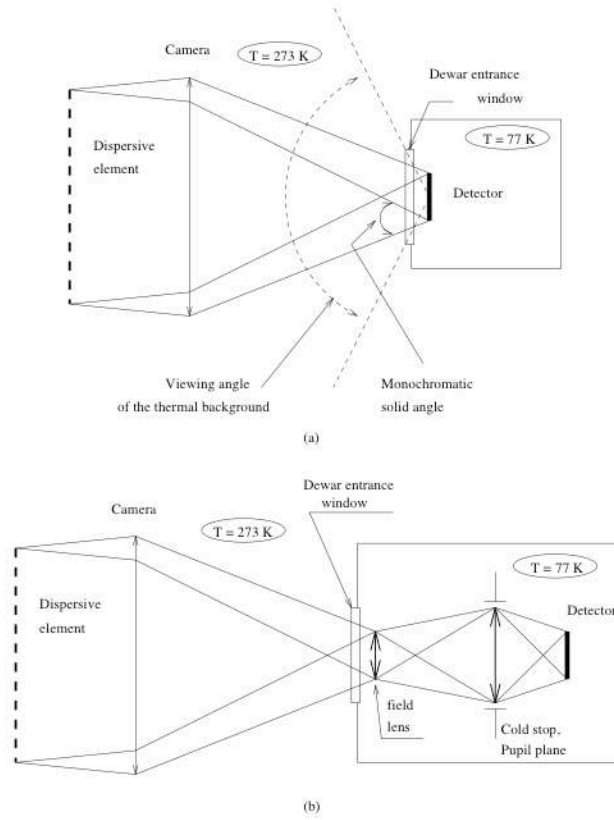
Figure 2. Schematic of the beams incident on a detector. The dispersive optics is non–cooled. (a): CCD–like implementation. (b): White pupil and cold stop

generates an 'integrated' thermal background. Hence, the penalty in not cooling the spectrograph is three-fold, by order of increasing importance:

1. slightly higher detectivity of the thermal background photons, converted in electrons through the sole detector + cold optics quantum efficiency, whereas with a cooled instrument the background photons are converted through the whole instrument efficiency.

2. a five to ten-fold increase in emissivity of the room temperature blackbody (i.e. up to 100%).

3. no dispersion of the background.

In consequence, the thermal background in the non-cooled case is given by the following expression, which does not depend anymore on the spectral resolution:

$$N^{\mathrm{TB}} = A\,\Omega\,\int \eta_{\mathrm{det}}\mathcal{F}(\lambda)\frac{2c}{\lambda^4\,\exp\frac{hc}{\lambda kT}-1}\,\mathrm{d}\lambda \tag{2}$$

with η_{det} the efficiency of the detector (+ the cold optics inside the detector camera). Minimizing the thermal background requires to minimize the étendue $A\,\Omega$ onto the detector.

3.2. Background étendue and detector implementation

To start our discussion, we consider the simplest detector implementation, as shown in figure 2 a. The whole optical train, collimator, dispersive element and camera is 'warm'. In such a case, the background is observed at a solid angle set by the diameter of the dewar entrance window and its back focal distance to the detector. Though quite dependent upon the camera design and instrument, sampling considerations lead with large telescopes and small

	J band [1.0 − 1.4]μm	H band [1.4 − 1.8]μm	K band [2.0 − 2.4]μm
(a)	∼ 0.3	∼ 720	∼ 6.2 10^5
(b)	∼ 0.02	∼ 55	∼ 4.7 10^4

Table 1. Thermal background levels in photons s^{-1} pixel^{-1} at 273 K in the J, H and K bands in situations similar to those of figure 2. The 'thermal' solid angle in case (a) has been taken equal to π (half cone angle of 60°), and we assume 18.5 μm pixels. In case (b), the étendue is 7.5 10^{-11} m^2 sr, corresponding to sampling 0.5 arcsec per pixel on a 4 meter telescope.

pixel sizes to short back focal distances and fast beams. For our purpose, we consider that the detector sees the external 'warm' environment under a beam speed of ∼ f/0.5, whereas the actual speed of the monochromatic beams is much slower. Table 1 shows the background flux in the near infrared bands under such a severe case (case (a)).

From these values, we derive that:

1. Implementing IR arrays barely like CCDs is at the limit of what is acceptable in the J band *in spectroscopy*, while this is not possible in the H band as the thermal background would dramatically dominate other photon sources. This is however a possible implementation scheme in broad-band *imaging*: the sky is then still the dominant source of photons, as it contributes in H to ∼ 7000 photons s^{-1} m^{-2} arcsec^{-2} band^{-1} (Ref. 3), i.e. ∼ 2000 photons s^{-1} pixel^{-1} on a 4 m telescope with 0.5 arcsec pixel^{-1} sampling and an overall efficiency of 10%. This CCD–like implementation is not a valid concept in the K band, even in broad-band imaging.

2. Minimizing the thermal background requires that it is seen by the detector at the same angle as the monochromatic beams. This leads to the double requirement to have a white pupil design as far as spectroscopy is concerned, and to image this white pupil into the dewar on a cold stop. This situation is depicted in figure 2 (b). The thermal background is reduced accordingly, as indicated in table 1, case (b).

3. The filters must be cold for operation in the J and H bands, if the detector is sensitive in the K band. 'Warm' J or H filters in front of the dewar, would generate thermal fluxes of several 10^4 to 10^5 photons s^{-1} pixel^{-1} in K.

In conclusion, implementing an IR array like a visible CCD is possible if limited to the sole J band, and provided that the J filter is cold. This however requires an efficient rejection of the thermal photons in H (a few 10^3) and in K (a few 10^6). Accessing the H band, or part of it, is still possible in spectroscopy, provided that a white pupil is imaged onto a cold stop. Here again, this requires an efficient rejection of the thermal photons in the K band, as we show in the next section.

3.3. Filter rejection in the K band

We assume that a near infrared detector is sensitive over the whole [1.0–2.5] μm region. This is the case for near infrared detectors in HgCdTe, whereas InGaAs has a cutoff wavelength of 1.7 μm.[6] As shown in the previous section, the filters must be cooled.

We have investigated the thermal background leakage in the wings of the J and H filters of the CFHT Redeye camera. For this, we have measured 'dark' currents through the J and H filters alone and in series with a thermal blocking filter (cutoff wavelength of 1.9 μm). Fortunately, the CFHT Redeye camera has two filter wheels and provides this double-filtering facility.

Figure 3 shows the residual thermal background up to 2.5 μm through the wings of the J and H filters as simply computed from their transmission curves. The noise in the figure comes from the noise in the transmission measurements. The thermal background in both the J and H filters is clearly affected by the leakage in the K band. Table 2 shows the thermal background values, as derived from figure 3 and from real measurements, with and without the thermal blocking filter. The differences between the predicted values in photons s^{-1} and the measured values in electrons s^{-1} are due to the quantum efficiency of the detector, plus the transmission of the cold optics
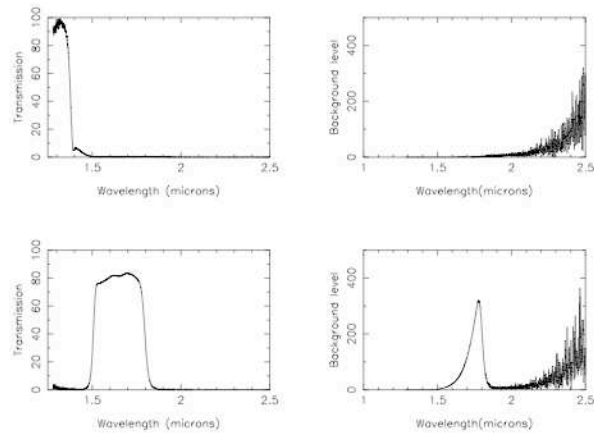
Figure 3. Thermal background through the J and H filters of the CFHT Redeye camera. Left: filter transmission curves. Right: transmission curves multiplied by a blackbody spectral distribution (in photons s^{-1} pixel^{-1} micron^{-1}). The étendue taken for this computation corresponds to the configuration of our observations. Up: J filter, down: H filter.

	J	H	
Predicted, wings included	20	50	photons s^{-1} pixel^{-1}
Predicted, wings excluded	$\ll 1$	34	photons s^{-1} pixel^{-1}
Measured, without thermal blocker	8	30	e$^-$ s^{-1} pixel^{-1}
Measured, with thermal blocker	2	20	e$^-$ s^{-1} pixel^{-1}

Table 2. Predicted and measured background fluxes in the J and H bands. The predicted fluxes are computed by integration of the curves in figure 3, assuming a blackbody radiation at 273 K, an emissivity of 100 per cent, and accounting for the étendue of our observations. The difference between the predicted values in photons s^{-1} and the measured values in e$^-$ s^{-1} are due to the quantum efficiency of the detector plus the transmission of the camera optics, including the filters. In the J band, the value measured with the blocking filter corresponds to the detector dark current. For the H filter, the results are consistent with a detector (plus cold optics) efficiency of $\sim 50\%$.

inside the camera. The observed increase of the background levels due to the leakage in the wings is in satisfactory agreement with the predicted one. A more detailed comparison would require a precise knowledge of the detector spectral sensitivity, especially between 2.4 μm and 2.5 μm. From table 2, it turns out that the use of a blocking filter used in series with the standard photometric filters are mandatory for a correct rejection of the thermal background in the K band. There is however a penalty of a few per cent in efficiency.

The rejection factor in the K band of the J and H filters of figure 3 is $\sim 3000 - 5000$. Getting rid of the requirement for the blocking filter would require filters with much higher rejection. Obviously, using a detector with a response cutoff wavelength of λ 2.0 μm would also allow to avoid this double filtering.

3.4. Thermal background subtraction

The subtraction of the thermal background can be done in two different ways:

1. via dark exposures, as usually done in the visible. Since the background consists in a complex pattern resulting from the temperature(s) of the local environment, the shutter should if possible be located as far as possible from the detector, for instance before the slit plane. Hence, most of the warm environment seen by the detector is identical to the one measured during an object exposure.
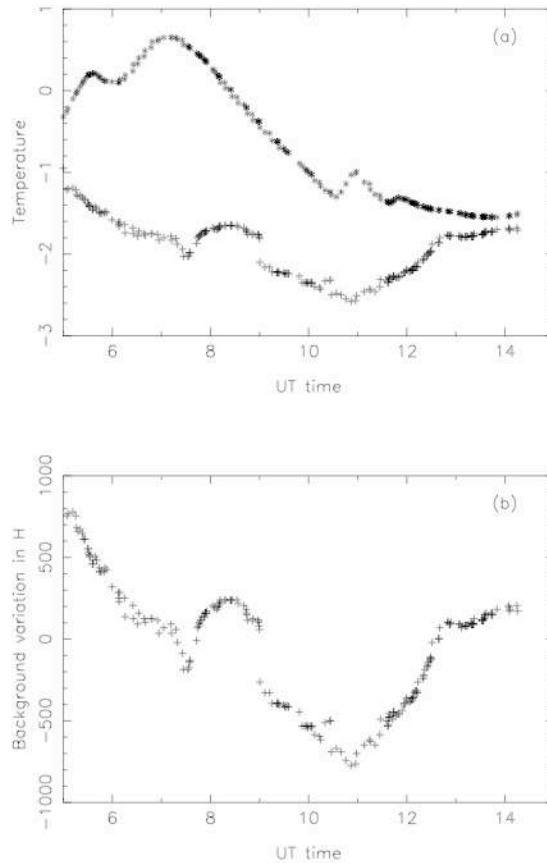
Figure 4. Temperature variations during a night in the CFHT dome (a), and corresponding variations of the thermal background (b). The upper curve shows the temperature variation during one night at two locations inside the dome. Crosses are for the air temperature six feet above the dome floor, stars are for the floor temperature by the telescope south pier, close to where the instrument was installed. In (b), we have computed the induced background variations, assuming arbitrarily that the instrument viewed a temperature blackbody corresponding to one of the above temperatures.

2. via beam switching exposures. In such a case, the thermal background is automatically removed together with the sky. There is a priori no need for specific 'dark' exposures.

Figure 4a shows the variations during a night of the ambient temperature as recorded at different locations inside the CFHT dome (these temperatures are logged in the image FITS headers).

We did not have enough clean 'dark' exposures in our data (which were in addition affected by bias instabilities) to carry out a proper correlation of the background level with ambient temperature. Moreover, as it is clear from figure 4a, various temperatures inside the dome are poorly correlated between themselves. It is then unlikely that any temperature measurement can be a good estimator of the blackbody temperature seen by the instrument.

Hence, we simply computed, from figure 4a, the background in H corresponding to one of the temperatures. The result is shown in figure 4b, assuming a 5 min exposure time in our observing conditions (same étendue). The mean background is in this case $\sim 10,000$ photons pixel^{-1}. The result is quite impressive, demonstrating that variations
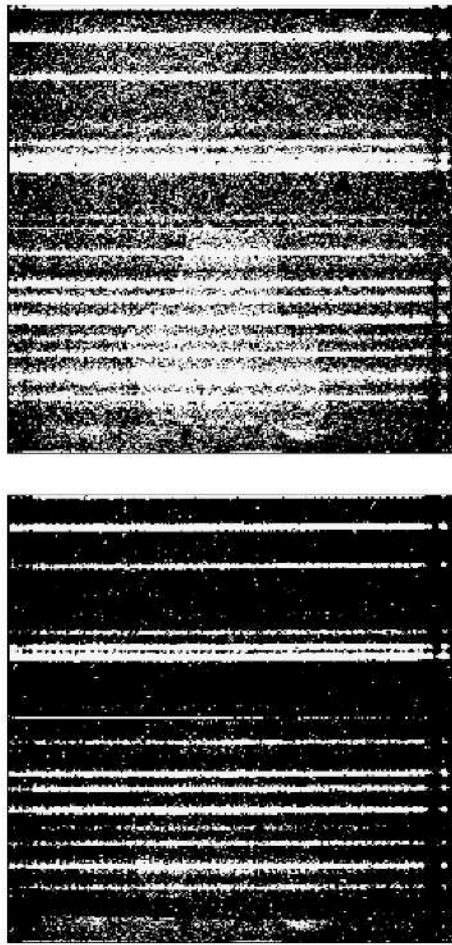
Figure 5. An example of ad'hoc background subtraction. One 'dark' exposure of 300 s is used for subtraction to 6 stacked 300 s sky images. Up, the 'dark' image was scaled by a factor 6 before subtraction, leaving a clear positive residual. Down, the same 'dark' image was scaled by a factor 6.3. Both images are displayed with the same cuts. The reduction and almost perfect cancellation of the background is clearly visible, though the sky image and the scaled background image correspond, after ad'hoc scaling, to different integration times. Clearly visible on the figure are the OH emission lines (along the y axis) and the fiber pattern (along the x axis).

up to 15 % of the background can be observed in a few hours, leading to background variations of several hundreds of photons per pixel and per exposure, i.e. much above the readout noise and sky + background shot noise.

However, these dramatic changes in the background level should not be considered as first order noise sources. Incorrect background subtraction typically leaves onto the detector a bias level that can be estimated on regions un-exposed by the sky light onto the detector. Such a local estimation may be used to scale a reference background image, improving the accuracy of the subtraction. Figure 5 illustrates this technique. However, using such 'blank' regions to scale the background may not be perfect, as such regions may also be used for sampling scattered light (see e.g. Ref. 7 for a scattered light subtraction recipe in multi-fibre spectroscopy).

Beam switching procedures allow a direct – and potentially better – subtraction of the background. However, the beam switching frequency may well be too low in comparison to the temperature time variations visible on figure 4a, and may need further processing as explained above using dark regions on the images. This again requires to take some specific background exposures, although these exposures are a priori not needed when using beam switching.

	4 m	4 m	8 m	8m	
	0.15	0.5	0.15	0.5	arcsec pixel−1
[1.4–1.80] μm	5	55	20	220	
[1.4–1.70] μm	1	10	4	45	
[1.4–1.65] μm	0.4	4	2	20	
[1.4–1.60] μm	0.2	2	0.6	7	
Sky (R $\sim$ 400)	15	160	60	660	

Table 3. Thermal background (T = 273 K) and sky fluxes in photons s^{-1} pixel^{-1} for different sampling conditions on 4 m and 8 m telescopes. The thermal background values may be converted in electrons s^{-1} pixel^{-1} by multiplying by the detector quantum efficiency, the cold optics transmission and the filter transmission. The sky values must be converted by multiplying by the overall atmosphere + telescope + instrument efficiency. The filter transmission curves are assumed perfectly rectangular with zero transmission outside the bandpass. It is also assumed that a white pupil is imaged onto a cold stop.

In conclusion to this analysis, the temperature variations during a night induce background variations which, if not properly handled, lead in turn to noise levels that largely exceed other noise sources. Taking dark exposures at the beginning and at the end of the nights for a simple subtraction – as usually done in the visible – is totally unrealistic. Special procedures have to be taken while observing for regularly sampling the background, and at the data reduction level for fine corrections allowing to properly subtract it.

3.5. Filtering the H thermal background

As it turns out from the previous discussions, the H band is actually a 'thermal' band in non-cooled near infrared spectroscopy. However, limiting the spectral range down to 1.8 μm allows to recover full performances in this band, at the expense of some spectral coverage. This is a pure translation of the situation occurring in the K band in imaging which has led to develop the well-known K' filter.[8]

Designing an H' filter cutting down the upper wavelengths of the H band of course depends on the spectrograph characteristics. For the sake of simplicity, we consider hereafter two cases, corresponding to realistic situations on 4 m and 8 m telescopes.

Table 3 shows the thermal background fluxes corresponding to these situations in different spectral bandpasses within the H band. Also indicated for reference are the mean sky fluxes, as computed from the data published in Ref. 3, assuming a two pixel resolution of $\sim$ 400. These values must be compared to the dark current which is a few e^- min^{-1} pixel^{-1} on new generation IR arrays.

The requirement to cut down the spectral range in H is directly dependent on the spectral resolution. At low spectral resolution, as shown on figure 1 corresponding to a two pixel resolution of $\sim$ 400, there are few regions of pure continuum between the OH lines. Hence, the signal to noise ratio is governed by the line intensities, and the full H band can be used without a significant impact on the performances. At the opposite, at higher spectral resolution, it becomes possible to observe between the OH lines in regions where the sky continuum and / or the detector dark current dominate with cooled instruments, and then the thermal background becomes the dominant source of noise with un–cooled instruments.

The use of linear filters, filtering the thermal background along the dispersion direction of the spectrograph, allows to further reduce the background. Linear filters (identical in the principle to the well–known Circular Variable Filters), can have spectral resolutions up to $\sim$ 100. Linear filters have in the present circumstance the very important advantage of significantly reducing the background at wavelengths below the cutoff wavelength. For instance, if the cutoff wavelength is 1.8 μm, the part of the spectrum close to 1.6 μm will see a background integrated over the range [1.59–1.61] μm, assuming a resolution of the linear filter of 80, instead of the background integrated over the range [1.5–1.8] μm without linear filter. Clearly, linear filters must be placed close to the detector, in an image plane, and not in a pupil plane.
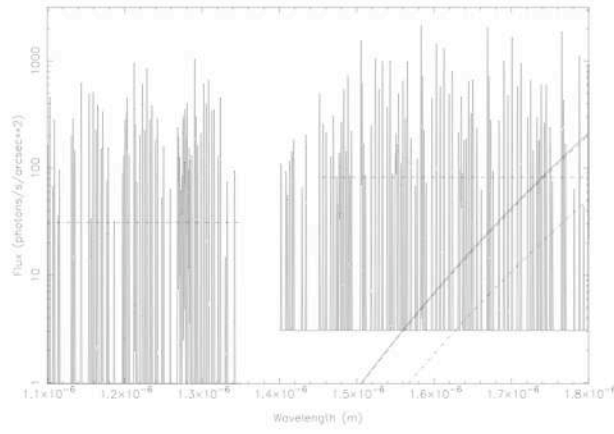
Figure 6. Spectral energy distribution of the sky and thermal backgrounds at a spectral resolution of 4000 per pixel. Same other parameters as in figure 1. The solid line indicates the background integrated from 1.0 μm to the wavelength reported along the horizonthal axis. The dashed line indicates the background integrated with a linear filter of resolution 10, and the dot–dashed line with a linear filter of resolution 100.
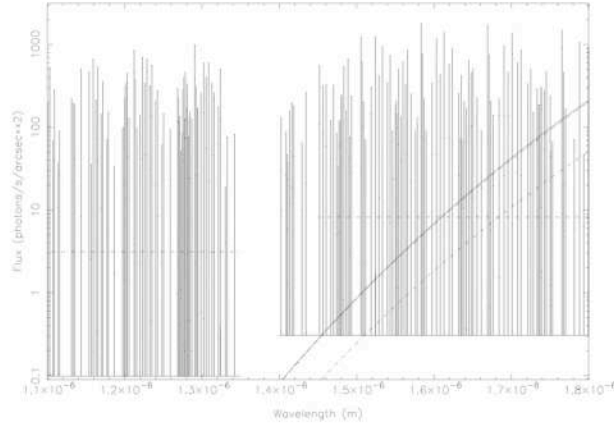
Figure 7. Same as figure 6 for a spectral resolution of 40000 per pixel.

Figure 6 and 7 demonstrate the impact of the background in non–cooled spectroscopy at high spectral resolution. From these figures, it turns out that working at a resolution of $\sim$ 2000 (two pixels) requires to limit the spectral range at $\sim$ 1.6 μm to keep sky–limited performances, whereas at a two pixel resolution of 20000, the thermal background is totally dominating. The use of linear filters, however, allows to increase the cutoff wavelengths by filtering the thermal background along the dispersion direction. The thermal background still dominates at wavelengths above $\sim$ 1.6 μm at R $\sim$ 2000 if the resolution of the linear filter is 10, but it now selectively affects the signal with wavelength, unlike without linear filter. Increasing the resolution of the linear filter to 100 allows to decrease the background by a factor of $\sim$ 4 at the cutoff wavelength.

3.6. Influence of the site temperature

The thermal background is obviously dependent on the site temperature. The dependence around 1.8 μm at 273 K on the number of thermal photons is:

$$N(T) \propto \exp(0.107 \times \Delta T) \tag{3}$$

where $N(T)$ is the number of thermal photons as a function of temperature and ΔT is the temperature variation.

This relation shows for instance that the thermal background in H at Paranal (VLT site, mean annual temperature: 12.6 °C) is $\sim$ 4 times higher than in Hawaii (mean annual temperature: 0 °C). On sites with high seasonal temperature variations, observing in winter time may significantly reduce the thermal background.

4. SKY CONTINUUM EMISSION IN J AND H: UPPER LIMITS

Ref. 9 and Ref. 10 give OH line wavelengths and intensities in the J, H and K bands. The emission lines are shown to be useful spectral calibrators for low to moderate resolution spectroscopy. Ref. 10 also provides a study of the time variations of the line intensities, and the authors derive a recipe for optimizing the exposure time according to these temporal variations. An important point is that no spatial variation over arcminute scales seem to exist. The continuum level between the OH lines has been measured by several authors, in view of OH airglow suppression instruments.[3,2]

We have attempted to measure the continuum level between the OH lines. From our observations taken at a spectral resolution of ~ 1500, we do not detect any continuum in the J band in a region free of lines, namely between 1.24230 and 1.24827 μm (wavelengths in vacuum, Ref. 11). We however derive an upper 3 σ limit of the continuum of ~ 300 photons s^{-1} m^{-2} arcsec^{-2}. This continuum upper limit is consistent with the value adopted in Ref. 2 from data published elsewhere. This represents a fraction of less than 2% of the mean sky in the J band ($\sim 17,000$ photons s^{-1} m^{-2} arcsec^{-2} (Ref. 3)).

We have performed the same analysis in the H band, and were not able either to detect with high confidence any continuum. We however derive a 3 σ upper limit of ~ 800 photons s^{-1} m^{-2} arcsec^{-2}, perfectly in agreement with the measurements reported in Ref. 3. This continuum upper limit has been estimated between the OH lines at 1.66110 and 1.66921 μm, and 1.67636 and 1.68405 μm (wavelengths in vacuum, Ref. 11). The first domain is the same as the one used in Ref. 3 for the detection of the continuum between the OH lines.

5. APPLICATIONS OF NON–COOLED NEAR INFRARED SPECTROSCOPY

5.1. Multiobject spectroscopy

Among the most rewarding applications of non–cooled near infrared spectroscopy is multi-object spectroscopy. This could be achieved either with mask or fibre systems as in the visible. Using masks with cryogenic instruments is unrealistic, as this would require frequent warming up / cooling down cycles for exchanging the masks.

One instrument has been developed at CFHT for multi-object spectroscopy in the J and H bands on the principle described in this paper. This instrument, OSIS, is an upgrade of the SIS way of the MOS–SIS instrument.[12] The instrument covers a huge spectral range, from ~ 400 nm to ~ 1800 nm. Switching from visible to near infrared wavelengths is done by manually exchanging the visible and infrared cryostats. A tip-tilt mirror allows to improve image quality in all the visible and infrared modes. The multiplex capability with 10 arcsec long slits can be as high as 12. Subsequent use of detectors of larger areas will allow to further improve this multiplex capability.

A dedicated IR instrument, with much wider field and massive multi–object capability (up to ~ 200), NIRMOS, is being developped for the VLT. It is the counterpart of VIMOS, operating in the visible.[13]

The use of linear filters, as described in section 3.5, has restricted applicability here, since the slits have variable locations in the focal plane. Therefore, the linear filter shall have a resolution small enough to allow for this variation in position of the slits. In practice, for NIRMOS, slits have to be laterally positioned within 0.5 to 1 arcmin to allow enough flexibility in the selection of the objects. This corresponds to 150–300 pixels, at a resolution of ~ 1.5 Angstroms per pixel. This limits the maximum resolution of the linear filter in H to ~ 30–60. The background at 1.8 μm is decreased accordingly by a factor 1.7 to 2.6.

5.2. Near infrared fibre spectroscopy

Though fibres have been used in visible spectroscopy for a long time, their application in the near IR has been quite limited up to now. In addition to ISIS IR,[4] fibres have been used in the IR either for interferometric applications[14] or plug plate–based multi–object spectroscopy at UKIRT. The interferometric applications are quite specific, and use monomode fibers.

At UKIRT,[15] the fibres feed a cryogenic spectrograph (CGS4), which allows to use the technique up to the K band, although with some degradation of the performances due an increase in thermal background. Two sets of fibres are available, silica fibres on one hand for the J and H bands, and zirconium fluoride fibers on the other hand for the K band.

For non–cooled IR spectroscopy, and if resorting to long fibre lengths, the logical approach is to use 'dry' silica as the material of choice, as it provides extremely good transmission performances over quite long distances (figure 8),
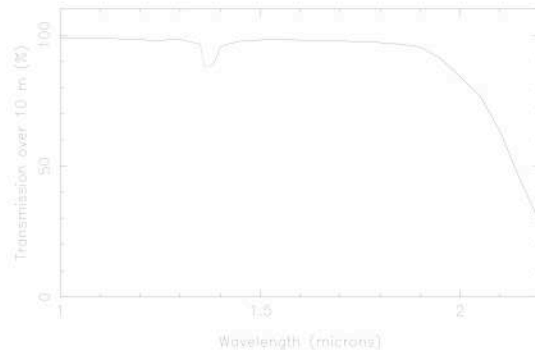
Figure 8. Transmission of dry silica over 10 meters. There is a small absorption in coincidence with the atmospheric absorption band between the J and H band. Silica is perfectly suited for the J and H bands over long fibre lengths.

up to 1.8 μm, matching exactly the cutoff wavelength of the technique described in this paper. Resorting to more exotic, fragile and expensive IR materials is in this case useless.

ACKNOWLEDGMENTS

REFERENCES

1. A. Tokunaga *Astrophys. and Space Science* **160**, p. 333, 1988.
2. T. Herbst *PASP* **106**, p. 1298, 1994.
3. T. Maihara, F. Iwamuro, T. Yamashita, D. Hall, L. Cowie, A. Tokunaga, and A. Pickles *PASP* **105**, p. 940, 1993.
4. R. Dallier, J. Cuby, J. Czarny, and J. Baudrand in *Infrared Astronomy with Arrays: the Next generation*, I. M. Lean, ed., p. 343, Kluwer Academic, 1994.
5. D. Simons, C. Clark, J. Kerr, S. Massey, S. Smith, and D. Toomey *Proc. SPIE* **1946**, p. 502, 1993.
6. M. Cohen and G. Olsen *Proc. SPIE* **1946**, p. 436, 1993.
7. R. Wyse and G. Gilmore *MNRAS* **257**, p. 1, 1992.
8. R. Wainscot and L. Cowie *ApJ* **103(1)**, p. 332, 1992.
9. E. Oliva and L. Origlia *A & A* **254**, p. 466, 1992.
10. S. Ramsay, C. Mountain, and T. Geballe *MNRAS* **259**, p. 751, 1992.
11. A. Steed and D. Baker *Appl. Opt.* **18**, p. 3386, 1979.
12. O. Le Fèvre, D. Crampton, P. Felenbok, and G. Monnet *A & A* **282**, p. 325, 1994.
13. O. Le Fèvre et al. *Proc. SPIE* **These proceedings**, 1998.
14. V. C. du Foresto, G. Mazé, and S. Ridgway *ASP Conference Series* **37**, 1993.
15. R. Haynes, R. Sharples, and K. Ennico *spectrum, Newsletter of the Royal Observatories* **7**, 1995.